Theory of self-assembly of microtubules and motors

Igor S. Aranson[1] and Lev S. Tsimring[2]
[1]*Argonne National Laboratory, 9700 South Cass Avenue, Argonne, Illinois, 60439, USA*
[2]*Institute for Nonlinear Science, University of California, San Diego, La Jolla, California 92093-0402, USA*
(Received 23 December 2005; revised manuscript received 7 August 2006; published 26 September 2006)

We derive a model describing spatiotemporal organization of an array of microtubules interacting via molecular motors. Starting from a stochastic model of inelastic polar rods with a generic anisotropic interaction kernel, we obtain a set of equations for the local rods concentration and orientation. At large enough mean density of rods and concentration of motors, the model describes an orientational instability. We demonstrate that the orientational instability leads to the formation of vortices and (for large density and/or kernel anisotropy) asters seen in recent experiments. We derive the specific form of the interaction kernel from the detailed analysis of microscopic interaction of two filaments mediated by a moving molecular motor and extend our results to include variable motor density and motor attachment to the substrate.

DOI: 10.1103/PhysRevE.74.031915 PACS number(s): 87.16.−b, 05.65.+b

I. INTRODUCTION

One of the most important functions of molecular motors is to organize a network of long filaments (microtubules) during cell division to form cytoskeleton of daughter cells [1]. In order to understand the details of this complex self-organization process, a number of *in vitro* experiments were performed [2–7] to study interaction of molecular motors and microtubules in isolation from other biophysical processes simultaneously occurring *in vivo*. At large enough concentration of molecular motors and microtubules, the latter organize in *asters* and *vortices* depending on the type and concentration of molecular motors.

In the above experiments the following qualitative picture of motor-filament interaction has emerged. After a molecular motor binds to a microtubule at a random position, it marches along it in a fixed direction until it unbinds without appreciable displacement of microtubules (since the mass of a molecular motor is small in comparison with that of the microtubule). However, if a molecular motor binds to *two* microtubules (most molecular motors have at least two binding sites), it can change their mutual position and orientation significantly [8]. In small-scale simulations [5], the interaction of rodlike filaments via motor binding has been studied and patterns resembling experimental ones were observed. In [9], a phenomenological model for the molecular motor density and the microtubule orientation has been proposed. The model included transport of molecular motors along microtubules and alignment of microtubules mediated by molecular motors. Simulations showed that vortices and asters indeed form in this model; however, only one large vortex formed in case of high density of motors. Reference [10] generalized this model by including separate densities of free and bound molecular motors, as well as the density of microtubules. This model exhibited a transition from asters to vortices as the density of molecular motors is increased, in apparent disagreement with experimental evidence [7] that asters give way to vortices with *decreasing* the molecular motors concentration. Somewhat similar approach was employed more recently by Sankararaman *et al.* [11] who introduced the additional mechanism of tubule alignments due to the gradient of the bound motor concentration. The introduction of this mechanism prevents single vortex formation at large motor densities obtained in Ref. [9]; however, it also strongly favors asters: lattices of vortices could only be obtained in the absence of the corresponding term in the equation for the vector field. A phenomenological flux-force relation for active gels was introduced in [12,13]. Although vortex and aster solutions were obtained in a certain limit, an analysis of that model is difficult because of the large number of unknown parameters and fields.

In Ref. [14], a set of equations for microtubules density and orientation was derived from conservation laws for microtubules probability distribution function. These conservation laws were based on the phenomenological expressions for the probability fluxes due to diffusion and motor-mediated interactions. The latter, however, assumed that tubules are only displaced and rotated infinitesimally in individual interactions, which may not be the case in experiments. The model does not produce the onset of spontaneous orientation for any density of microtubules. The authors argue that asters and vortices may be created as a result of the "bundling instability" [15]. However, this model demonstrated the bundling instability at small densities of tubules and oscillatory orientational instability at large densities contrary to observations in which the orientational ordering is observed at smaller densities and is not oscillatory. In subsequent publication [16], a derivation of the probability conservation equations from microscopic mean-field model of forces between tubules and motors was presented; however, the assumptions made in the course of derivation (i.e., infinitely stiff molecular motors) lead to a surprising conclusion that filaments do not change their orientation during interaction.

In this paper we present an alternative calculation of the microscopic motion of two filaments connected by a moving motor in a viscous fluid and show that filaments do change orientation as a result of the interaction. In our short publication [17], we derived a continuum model for the collective spatiotemporal dynamics of microtubules starting with a stochastic microscopic master equation for interacting inelastic polar rods, assuming that the density of molecular motors is homogeneous in space. Our model differs from the transport

equations [14] in that it treated the interaction between two tubules as an instantaneous inelastic "collision." Although an elementary interaction may change the orientation of the two filaments significantly (in the limiting case of completely inelastic collision they become parallel), after a motor detaches from the tubules, they drift apart both in physical and angular space due to thermal fluctuations. The nontrivial patterns may emerge as an interplay between the tubule-tubule interaction and fluctuations-driven relaxation. The model indeed exhibits an onset of orientational order for large enough density of microtubules and molecular motors [18], formation of vortices, and then asters with increase in the molecular motors concentration, in a qualitative agreement with experiment.

In this paper we present a more detailed derivation of our equations, starting from a microscopic model of tubule-motor interaction. In addition to our previous findings in Ref. [17], we considerably extended our analysis in a number of directions.

(i) We derived the interaction kernel from microscopic rules and related the kernel characteristics with the properties of the motors taken from available experimental data.

(ii) We considered the situation when a fraction of molecular motors are attached to a substrate (usually, a glass plate). This modification allowed as to improve an agreement with experiment. In particular, interaction with the substrate explains slow rotation of vortices and suppression of the density in the vortex cores, as observed in experiments [4,5].

(iii) We lifted the assumption of the homogeneous distribution of molecular motors and included an additional equation for the evolution of the molecular motor density. Our results show that variable motor density does not qualitatively change the phase diagram and the structure of the solutions, indicating that motor transport is not a *primary* mechanism of self-organization, contrary to assumptions of Refs. [9–11].

The structure of the paper is as follows. In Sec. II, we present a kinetic description of inelastically interacting polar rods and derive a model equation for the mean orientation for a Maxwell model of tubule-tubule interaction. In Sec. III, we calculate the form of the interaction kernel from microscopic rules of interaction of two filaments. In Sec. IV, we reduce the kinetic equations for the tubule probability distribution function to the set of partial differential equations for local orientation and density of microtubules. In Sec. IV A, the stability analysis of the isolated vortex and aster solutions is performed and the phase diagram of various regimes is presented as the function of motor density and anisotropy of the interaction kernel. In Sec. V, we include effects of motors attached to the substrate and explain rotation of the vortices and onset of large variations of the microtubules density. In Sec. VI, we consider effects of variable motor density and derive the equation for the evolution of the motors. Details of derivations are summarized in [19].

II. KINETIC THEORY OF INELASTIC POLAR RODS

A. Maxwell model for inelastic polar rods

At this stage, molecular motors enter the model implicitly by specifying the microscopic interaction rules between two rods. Since the diffusion of small motors is about two orders of magnitude higher than that of large and heavy microtubules, in this section we neglect spatial variations of the motor density and treat the collision rules as spatially homogeneous. Effects of variable motor density are considered in Sec. VI. For simplicity we consider the problem in the two-dimensional $x-y$ plane. Each rod is assumed to be of length l and diameter $d \ll l$, and is characterized by the position of its center of mass $\mathbf{r}$ and the unit vector $\mathbf{n}=(\cos\phi, \sin\phi)$ in the direction of its polar end (we specify that it is oriented at the angle ϕ to the x axis).

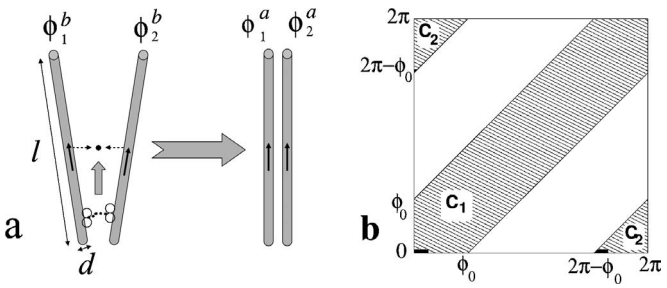

FIG. 1. (a) Sketch of motor-mediated two-rod interaction for fully inelastic collision ($\gamma=1/2$) and (b) integration regions $C_{1,2}$ for Eq. (2).

Let us first consider the orientational dynamics only and ignore the spatial locations of interacting rods (an analog of the Maxwell model of binary collisions in kinetic theory of gases; see e.g., [20]). We model the motor-mediated inelastic interaction by an instantaneous collision in which two rods change their orientations according to the following collision rule:

$$\begin{pmatrix} \phi_1^a \\ \phi_2^a \end{pmatrix} = \begin{pmatrix} \gamma & 1-\gamma \\ 1-\gamma & \gamma \end{pmatrix} \begin{pmatrix} \phi_1^b \\ \phi_2^b \end{pmatrix}, \tag{1}$$

where $\phi_{1,2}^b$ are the two rods' orientations before and $\phi_{1,2}^a$ after the collision, and the constant γ characterizes inelasticity of collisions (analog of restitution coefficient in granular media). The angle between two rods is reduced after the collision by an "inelasticity" factor $\varepsilon=2\gamma-1$. Totally elastic collision corresponds to $\gamma=0$ or $\varepsilon=-1$ (the rods exchange their angles), and a totally inelastic collision corresponds to $\gamma=1/2$ or $\varepsilon=0$: rods acquire identical orientation $\phi_{1,2}^a=(\phi_1^b+\phi_2^b)/2$ [see Fig. 1(a)]. Here we assume that two rods only interact if the angle between them before collision is less than some cutoff angle ϕ_0, $|\phi_2^b-\phi_1^b|<\phi_0<\pi$. Because of 2π periodicity, we have to add the rule of collision between two rods with $2\pi-\phi_0<|\phi_2^b-\phi_1^b|<2\pi$. In this case, we have to replace $\phi_1^{b,a}\to\phi_1^{b,a}+\pi, \phi_2^{b,a}\to\phi_2^{b,a}-\pi$ in Eq. (1). In the following, we will only consider the case of totally inelastic rods ($\gamma=1/2$) and $\phi_0=\pi$, the generalization for arbitrary γ and ϕ_0 is straightforward (see [19]). The probability distribution of orientation angles $P(\phi)$ obeys the following master equation:

$$\partial_t P(\phi) = D_r \partial_\phi^2 P(\phi) + g \int_{C_1} d\phi_1 d\phi_2 P(\phi_1) P(\phi_2) \times [\delta(\phi - \phi_1/2 - \phi_2/2) - \delta(\phi - \phi_2)] + g \int_{C_2} d\phi_1 d\phi_2 \times P(\phi_1) P(\phi_2) \Big[\delta\Big(\phi - \phi_1/2 - \tfrac{\phi_2}{2} - \pi\Big) - \delta(\phi - \phi_2) \Big], \quad (2)$$

where g is the "collision rate," or a probability of two tubules to interact via a motor, the diffusion term $\propto D_r$ describes thermal fluctuations of the rod orientation, and the integration domains C_1, C_2 are shown in Fig. 1(b). The collision rate is proportional to the concentration of molecular motors m, and from the dimensional analysis one finds that g is of the order of $mD_r l^2$, since $1/D_r$ is the only time scale in Eq. (2), and the effective interaction cross section of microtubules is of the order of l^2.

Rescaling time scale $t_s = D_r t$, probability $P_s = gP/D_r$, and defining angle difference $w = \phi_2 - \phi_1$, one obtains

$$\partial_t P_s(\phi) = \partial_\phi^2 P_s(\phi) + \int_{-\pi}^{\pi} dw \left[P_s\left(\phi + \frac{w}{2}\right) P\left(\phi - \frac{w}{2}\right) - P_s(\phi) P_s(\phi - w) \right] \quad (3)$$

(we dropped the subscript s at time t for brevity). The rescaled number density $\rho = \int_0^{2\pi} P_s(\phi,t) d\phi$ now is proportional to the *density of rods multiplied by the density of motors*. In Sec. II B, an increase of the density of molecular motors is reflected in our analysis as an increase of the number density ρ.

B. Orientation transition

Equation (3) possesses uniform steady-state solution $P(\phi) = P_0 = \rho/2\pi = \text{const}$ corresponding to isotropic distribution of rods. This solution loses its stability with respect to anisotropic perturbations with the increase of density ρ. The instability signals the onset of spontaneous orientation. Substituting solution to Eq. (3) in the form $P(\phi,t) = P_0 + \xi(\phi,t)$, where ξ is small perturbation, we obtain linear equation for ξ

$$\partial_t \xi(\phi) = \partial_\phi^2 \xi(\phi) + \frac{\rho}{2\pi} \int_{-\pi}^{\pi} \left[\xi\left(\phi + \frac{w}{2}\right) + \xi\left(\phi - \frac{w}{2}\right) - \xi(\phi - w) - \xi(\phi) \right] dw. \quad (4)$$

Looking for the solution to Eq. (4) in the form $\xi \sim \exp[\lambda_k t \pm ik\phi]$, where the azimuthal wave number $k \neq 0$ is an integer, for the growth rate λ_k we find

$$\lambda_k = \rho \left[\frac{4}{k\pi} \sin\left(\frac{\pi k}{2}\right) - 1 \right] - k^2. \quad (5)$$

Thus, it follows from Eq. (5) that perturbations with $k = \pm 1$ have the largest growth rate $\lambda_1 = \rho(4/\pi - 1) - 1$. The instability ($\lambda_1 > 0$) occurs for the density $\rho > \rho_c = \pi/(4-\pi) \approx 3.662$ and leads to breaking the azimuthal symmetry and formation of anisotropic, i.e., oriented states. The resulting orientation is determined by initial conditions contained in the perturbation ξ.

C. Fourier expansion

Let us consider the Fourier harmonics of the probability density $P(\phi)$

$$P_k = \langle e^{-ik\phi} \rangle = \frac{1}{2\pi} \int_0^{2\pi} d\phi e^{-ik\phi} P(\phi,t). \quad (6)$$

The zeroth harmonic $P_0 = \rho/2\pi = \text{const}$, and the real and imaginary parts of P_1 represent the components of the averaged unit orientation vector $\mathbf{n}$: $\tau_x = \langle n_x \rangle = \langle \cos\phi \rangle$, $\tau_y = \langle n_y \rangle = \langle \sin\phi \rangle$. Note that $\tau_x + i\tau_y = P_1^*$. Substituting (6) into Eq. (3) yields

$$\dot{P}_k + (k^2 + \rho) P_k = 2\pi \sum_m P_{k-m} P_m S\left(\frac{\pi k}{2} - m\pi\right) \quad (7)$$

[here $S(x) = \sin x/x$]. Because of the rotational diffusion term, the magnitudes of high-order harmonics decay rapidly with k^2; see Eq. (5). Neglecting all P_k for $|k| > 2$, we obtain from Eq. (7)

$$\dot{P}_1 + P_1 = P_0 P_1 2(4 - \pi) - \tfrac{8}{3} P_2 P_1^* \quad (8)$$

$$\dot{P}_2 + 4P_2 = -P_0 P_2 2\pi + 2\pi P_1^2. \quad (9)$$

Since near the orientation transition threshold the decay rate of P_2 is much larger than the growth rate of P_1 [see Eq. (5)], we can neglect the time derivative $\dot{P}_2$ and obtain the relation $P_2 = 2\pi(\rho+4)^{-1} P_1^2$, which leads to the Landau-type equation for the average orientation vector $\boldsymbol{\tau}$

$$\dot{\boldsymbol{\tau}} = \epsilon \boldsymbol{\tau} - A_0 |\boldsymbol{\tau}|^2 \boldsymbol{\tau} \quad (10)$$

with constants

$$\epsilon = \rho(4\pi^{-1} - 1) - 1 \approx 0.273\rho - 1 = 0.273(\rho - \rho_c)$$

$$A_0 = \frac{16\pi}{3(\rho+4)} \approx 2.18 + O(\rho - \rho_c). \quad (11)$$

For large enough densities $\rho > \rho_c = 3.662$, an orientation transition (instability) leads to spontaneous rods alignment. This instability saturates at the value determined by the density ρ. Close to the threshold the constant $A_0 \approx 2.18$.

In order to verify our approximations, we solved Eq. (3) for the inelasticity parameter $\gamma = 1/2$ (or $\varepsilon = 0$) and the cutoff angle $\phi_0 = \pi$ numerically by the finite difference method. We find that random initial conditions rapidly evolved toward a single-peaked stationary distribution, the position of the maximum of the distribution being determined by initial conditions; see, for detail, [17]. We obtained that numerical solutions to Eq. (3) are consistent with the truncated model (10) up to densities $\rho < 5.5$ [17]. Recently, Ben-Naim and Krapivsky [21] developed analytical procedure for obtaining exact steady-state solutions to Eq. (3).

We also studied Eq. (3) for the cutoff angle $\phi_0 \neq \pi$, and for ϕ_0 close to π no qualitative difference was found. For the smaller ϕ_0 values, e.g., $\phi_0 < \pi/2$, since only almost parallel microtubules interact attractively, we often obtained long-living multiple peak distributions, with the number of peaks at different angles separated roughly by π/ϕ_0. This situation corresponds to coexistence of multiple microtubules clusters with different orientation angles ϕ_n. Although the distribution possibly relaxes toward a single peak, the transient time appears to be very large due to exponentially weak interaction between the clusters.

D. Spatial localization of tubule-tubule interaction

To describe the *spatial localization* of tubule-tubule interaction, we introduce the probability distribution $P(\mathbf{r},\phi,t)$ to find a rod with orientation ϕ at location $\mathbf{r}$ at time t. The equation for $P(\mathbf{r},\phi,t)$ in the original variables can be written as

$$\begin{aligned}\partial_t P(\mathbf{r},\phi) &= D_r \partial_\phi^2 P(\mathbf{r},\phi) + \partial_i D_{ij} \partial_j P(\mathbf{r},\phi) \\ &+ \int\int d\mathbf{r}_1 d\mathbf{r}_2 \int_{-\phi_0}^{\phi_0} dw \Bigg[W\left(\mathbf{r}_1,\mathbf{r}_2,\phi+\frac{w}{2},\phi-\frac{w}{2}\right) \\ &\times P\left(\mathbf{r}_1,\phi+\frac{w}{2}\right) P\left(\mathbf{r}_2,\phi-\frac{w}{2}\right) \delta\left(\frac{\mathbf{r}_1+\mathbf{r}_2}{2}-\mathbf{r}\right) \\ &- W(\mathbf{r}_1,\mathbf{r}_2,\phi,\phi-w) P(\mathbf{r}_2,\phi) P(\mathbf{r}_1,\phi-w) \\ &\times \delta(\mathbf{r}_2-\mathbf{r}) \Bigg] \end{aligned} \tag{12}$$

where $W(\mathbf{r}_1,\mathbf{r}_2,\phi_1,\phi_2)$ is the interaction kernel (a probability of two tubules with center mass positions $\mathbf{r}_1,\mathbf{r}_2$ and orientations ϕ_1,ϕ_2 to interact. This interaction kernel replaces the constant collision rate g entering the Maxwell model (2).

Unlike the Maxwell model equation (3), Eq. (12) contains two diffusion terms (translational and angular), and the motor-mediated tubule-tubule collision integral now contains an interaction kernel W, which depends on the relative tubule positions and orientations. Even though the system of microtubules interacting with molecular motors is nonequilibrium, we use the standard Einstein-Stokes relations for the rotational D_r and translational D_{ij} diffusion coefficients (in the original scaling) known from polymer physics [22]

$$D_r = \frac{4k_B T_e}{\xi_r}, \quad D_{ij} = D_\parallel n_i n_j + D_\perp(\delta_{ij} - n_i n_j)$$

$$D_\parallel = \frac{k_B T_e}{\xi_\parallel}, \quad D_\perp = \frac{k_B T_e}{\xi_\perp} \tag{13}$$

where $\xi_r, \xi_\parallel, \xi_\perp$ are corresponding viscous drag coefficients. For rigid rodlike molecules in fluid,

$$\xi_\parallel = \frac{2\pi\eta_s l}{\ln(l/d)}; \quad \xi_\perp = 2\xi_\parallel; \quad \xi_r \approx \frac{\pi\eta_s l^3}{3\ln(l/d)}, \tag{14}$$

where η_s is the shear viscosity [22]. The drag coefficients are slightly modified for thin films and membranes; see e.g., [23]. Note that we used in (13) the effective temperature T_e, which is mostly due to microtubule collisions and motor fluctuations. This effective temperature may exceed considerably the thermodynamic temperature T.

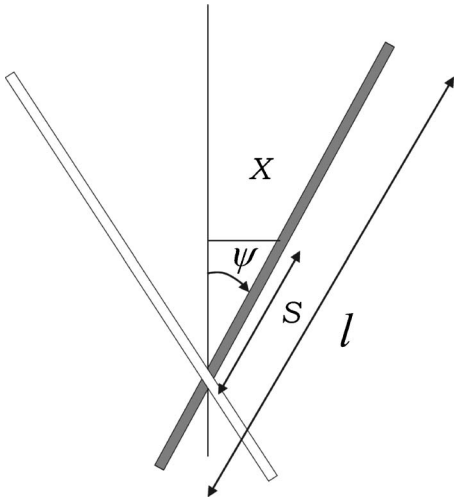

FIG. 2. Sketch of the interaction of two microtubules, S is the distance from the motor to the center point of microtubule.

The last term of Eq. (12) describes motors-mediated interaction of rods. In Sec. III, we present a detailed analysis of motor-mediated tubule-tubule interaction and derive the corresponding form of the interaction kernel W.

III. MICROSCOPIC PICTURE OF TUBULE-TUBULE INTERACTION

In order to develop a kinetic model of many interacting tubules, we need to introduce a more specific model of interaction between two tubules mediated by a molecular motor. Namely, we should specify the "collision rules," or a relationship between positions and orientations of two tubules before and after the interaction via motor attachment and/or detachment, and the collision rate, or the probability of the collision to occur given the positions and orientations of two tubules. The latter will play a role of interaction kernel in the corresponding master equation for the tubule probability distribution.

A. Collision rules

Here we specify these rules by integrating the equations of motion of the two tubules. This calculation is based on a number of simplifications. We assume that two infinitely rigid rods of equal length l interact with one molecular motor. We assume that the motor moves with constant speed V along the rods (the results can are trivially generalized for the case of $V \neq$ const). To simplify the system even further, we consider a symmetric case: the distance of the motor from the center point of the rod S, $-l/2 < S < l/2$ is the same for both rods; see Fig. 2. We choose the orientation of x axis along the bisector of the angle between the tubules, and we denote the angle between a tubule and a bisector ψ [note that $\psi = (\phi_2 - \phi_1)/2$]. Since the size of a motor ($\approx$30 nm) is much smaller than the length of a microtubule ($l \approx 5-10$ μm), we

consider a limit of zero motor size. Since the motor's bending elasticity is rather small, we approximate the motor by a soft spring and prescribe that the force F exerted on the tubules due to motor motion is perpendicular to the bisector of the angle between the tubules (i.e., along the motor), which in the symmetric case is along the x axis; see Fig. 2. Even if the symmetry is initially broken and the force is exerted at an angle to the x axis, the force will initiate a relative displacement of the tubules in the y direction, which will shift the binding points in such a way as to restore the symmetry.

The equations governing evolution of the angle ψ between the microtubule and the bisector and the coordinates X,Y of the center of mass of the microtubule are obtained from balance of torques and forces due to motor motion and viscous drag forces

$$\partial_t \psi = (\xi_r^{-1} S \cos\psi) F, \tag{15}$$

$$\partial_t X = (\xi_\parallel^{-1} \cos^2\psi + \xi_\perp^{-1} \sin^2\psi) F, \tag{16}$$

$$\partial_t Y = (\xi_\parallel^{-1} - \xi_\perp^{-1}) \sin\psi \cos\psi F. \tag{17}$$

Here $\xi_r, \xi_\parallel, \xi_\perp$ are rotational and translational viscous drag coefficients introduced earlier (14).

In the following, we neglect the anisotropy of the translation friction ($\xi_\parallel = \xi_\perp$ [24]), then the equations of motion will simplify considerably

$$\partial_t \psi = \xi_r^{-1} S \cos\psi F, \tag{18}$$

$$\partial_t X = \xi_\parallel^{-1} F, \tag{19}$$

$$\partial_t Y = 0. \tag{20}$$

Additional kinematic equation is obtained from the condition that the motor is attached at the distance S from the center of tubule, which gives

$$X = -S \sin\psi. \tag{21}$$

Differentiating Eq. (21) with respect to time and using condition $dS/dt = V$, we exclude the force F and derive an equation for angle ψ [note that the analysis in this section is also valid for arbitrary time-dependent velocity of the motor $V(t) > 0$]

$$\frac{d\psi}{dt} = -\frac{\kappa V S \cos\psi \sin\psi}{1 + kS^2 \cos^2\psi}, \tag{22}$$

where constant $\kappa = \xi_\parallel / \xi_r \approx 12/l^2$; see Eq. (14). We make the following substitutions: renormalized time $t_s \to \kappa S^2$ and variable $u \to \cos^2\phi$. In new variables, Eq. (22) can be written as

$$\frac{dt_s}{du} = \frac{1 + t_s u}{u(1-u)}. \tag{23}$$

Equation (23) is linear with respect to t_s and therefore has an exact solution

$$t_s = \frac{C + \ln u}{1 - u}, \tag{24}$$

where C is a constant determined by initial conditions. Returning to original variables, we obtain

$$\frac{C + \ln(\cos^2\psi)}{\sin^2\psi} = \kappa S^2. \tag{25}$$

For small angles ψ, Eq. (25) simplifies and we obtain

$$\psi = \psi_i \frac{\sqrt{1 + \kappa S_i^2}}{\sqrt{1 + \kappa S^2}}, \tag{26}$$

where the ψ_i, S_i are the angle and position of the interaction point at $t = 0$.

For the final angle ψ_f, which is acquired when the motor reaches the end of the microtubules ($S = l/2$), we derive

$$\psi_f = \psi_i \frac{\sqrt{1 + \kappa S_i^2}}{\sqrt{1 + \kappa l^2/4}}. \tag{27}$$

As one sees from Eq. (27), the final angle ψ_f depends on the initial angle ψ_i and the initial attachment position S_i. Assuming that the probability of attachment of the motor is independent of the position along the microtubule S, in the small ψ_i approximation, for average angle

$$\langle \psi_f \rangle = l^{-1} \int_{-l/2}^{l/2} \psi(S_i) dS_i, \tag{28}$$

we derive

$$\langle \psi_f \rangle = \psi_i \left[\frac{1}{2} + \frac{\operatorname{arcsinh}(\sqrt{\kappa l^2}/2)}{\sqrt{\kappa l^2}\sqrt{1 + \kappa l^2/4}} \right]. \tag{29}$$

Thus, the averaged change in the angle between two tubules, or the inelasticity factor $\varepsilon = \langle \psi_f \rangle / \psi_i$ is

$$\varepsilon = \frac{1}{2} + \frac{\operatorname{arcsinh}(\sqrt{\kappa l^2}/2)}{\sqrt{\kappa l^2}\sqrt{1 + \kappa l^2/4}}. \tag{30}$$

Obviously, for $\kappa l^2 \to \infty$ the inelasticity factor $\varepsilon \to 1/2$, which corresponds to (partly) inelastic collision between the rods. For the case of rigid rods, we obtain from Eq. (14) that $\kappa l^2 \approx 12$, which gives $\varepsilon \approx 0.67$, which is considerably greater than the fully inelastic case of $\varepsilon = 0$. With the increase of κ, the inelasticity factor ε slowly decreases (e.g., for $\kappa l^2 = 30$ we obtain $\varepsilon = 0.6$).

For arbitrary initial angles ψ_i, in order to find the average angle change we solved Eqs. (25) and (28) numerically (see Fig. 3). There is a week dependence of ε on the initial angle ψ_i. In a wide range of initial angles $0 < \psi_i < 0.75\pi$, the inelasticity factor $\varepsilon \approx 0.6$ and then $\varepsilon \to 1$ for $\psi_i \to \pi$.

In this section we have found that interaction of two rigid rods is only partly inelastic: the overall decrease in the initial angle does not exceed 40%. Certainly, there are additional physical mechanisms further increasing the inelasticity of interaction, such as (i) finite flexibility of microtubules, which may significantly reduce the factor ε. Investigation of this interesting problem we leave to future studies. (ii) Multiple motor attachment—obviously, if two or more motors attach

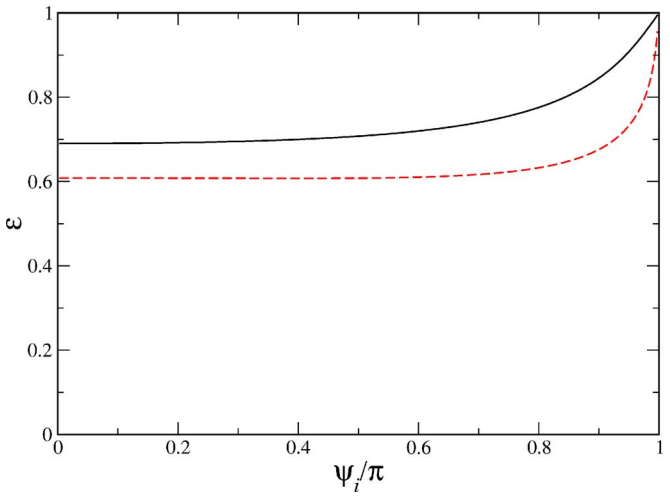

FIG. 3. (Color online) The effective inelasticity factor ε vs normalized initial angle ψ_i/π calculated from Eq. (28) for $\kappa=12/l^2$ (solid line). For comparison, ε at $\kappa=30/l^2$ is also shown (dashed line).

simultaneously at different positions to two microtubules, it should make them perfectly aligned, corresponding to fully inelastic collision $\varepsilon=0$. Consideration of this effect also goes beyond applicability of our analysis. Taking into account these considerations, we believe that the assumption of fully inelastic collisions between microtubules can be a reasonable approximation for flexible tubules and not too small motor density.

B. Collision rate

Now we turn to the calculation of the collision rate $W(\mathbf{r}_1,\mathbf{r}_2,\phi_1,\phi_2)$ between two tubules with center-of-mass positions $\mathbf{r}_1,\mathbf{r}_2$ and orientations $\mathbf{n}_1,\mathbf{n}_2$ (or angles ϕ_1,ϕ_2). We consider a translationally and rotationally invariant system, so the collision rate depends only on the position and orientation differences, $W(\mathbf{r},\phi)$, where $\mathbf{r}=\mathbf{r}_1-\mathbf{r}_2$, and, as before, $\psi=(\phi_1-\phi_2)/2$.

Microtubules interact via a motor attachment only if they intersect, which is expressed by the condition

$$|\mathbf{r}_1-\mathbf{r}_2|<\frac{l}{2}\sin\psi. \tag{31}$$

This gives the collision rate in the form

$$W=W_l\Theta\left(|\mathbf{r}_1-\mathbf{r}_2|-\frac{l}{2}\sin\psi\right), \tag{32}$$

where θ is the Θ function, and W_l is the linking rate, or the probability of two tubules to link via a motor given that they intersect. The latter is directly proportional to the concentration of molecular motors bound to a tubule. If the concentration of the motors along the tubules were uniform, the collision rate would be uniform inside the parallelogram defined by Eq. (32). However, due to the transport of motors along the tubules, their concentrations increase toward the polar ends of the filaments.

In order to compute the inhomogeneous motor distribution along a filament, we assume that the motors can be in two different states, bound and free. The concentration of free motors m_f is a function of the coordinate along the tubule S, $(-l/2<S<l/2)$, perpendicular coordinate $r_\perp$ (we consider a two-dimensional domain), and time t. Bound motors are localized on the tubule itself; thus, so their area concentration is $M_b(S,t)\delta(r_\perp)$.

The inhomogeneous motor distribution can be evaluated from the following microscopic equations for motor attachment and/or detachment and advection processes:

$$\partial_t m_f=(p_{\rm off}M_b-p_{\rm on}m_f)\delta(r_\perp)+D\nabla^2 m_f$$

$$\partial_t M_b=-p_{\rm off}M_b+p_{\rm on}m_f(S,0,t)-\partial_S(VM_b). \tag{33}$$

These equations, formulated in terms of the concentration of bound and/or free motors M_b,m_f, describe random binding and/or unbinding of the motors with the probabilities $p_{\rm on,off}$; diffusion of free motors (diffusion coefficient D), and the advection of bound motors with the velocity V along the tubule. The parameter $p_{\rm off}$ characterizes processivity of molecular motors: large $p_{\rm off}$ corresponds to small processivity, motor unbinds soon after it binds to a filament.

According to experiments (see, e.g., [25]) multiple motors can be attached to a single tubule. However, for the sake of simplicity we assume that only one motor can be attached per elementary binding site, which represents a section of approximately $l_0=10$ nm along the tubule [26]. This leads to a hard-core repulsion, which in the simplest approximation can be taken into account by introducing local "pressure" p of bound motors, and modifying the transport speed V,

$$V=V_0-\eta\partial_S p, \tag{34}$$

where $V_0=$const is the velocity of individual motor (~ 1 μ/s) and η is an effective mobility. Pressure p diverges as the bound motor density M_b approaches densely packed limit of one motor per binding site $M_b\to M_0\sim 1/l_0$. We will adopt a simple generic expression for the pressure as a function of the bound motor density (see for comparison expressions for pressure in granular hydrodynamics near closed-packed density [27–29])

$$p=\frac{M_bT_m}{1-M_b/M_0}. \tag{35}$$

The "motor temperature" T_m (analog of a granular temperature) is determined by fluctuations of bound motors on the tubule and is typically small (see below), so the pressure gradient $\partial_S p$ can be neglected everywhere except where the density is very close to the dense limit.

In the stationary state Eqs. (33) assume the form

$$(p_{\rm off}M_b-p_{\rm on}m_f)\delta(r_\perp)+D\nabla^2 m_f=0 \tag{36}$$

$$-p_{\rm off}M_b+p_{\rm on}m_f(S,0)=\partial_S[V_0M_b-\eta M_b\partial_S p]. \tag{37}$$

Since the diffusion constant D of free motors is large, we can neglect the inhomogeneity in the free motor distribution and assume the constant density of free motors $m_f=$const in Eq. (37). Eq. (37) has to be solved with the

boundary condition $M_b=0$ at $S=-l/2$. At the end of the tubule $S=l/2$ the "exit" flux of bound motors VM_b is determined by the detachment probability p_{end} of the motor, resulting in the condition $VM_b=p_{\text{end}}l_0M_b$. For small T_m, the density of bound motors has two distinct phases: low-density "gas phase" near the beginning of the tubule ($S=-l/2$), and a high density "solid phase" near the end ($S=l/2$) [30]. The location of the boundary between these phases can be found by equating the fluxes of bound motors in the two phases. In the low-density phase, the pressure term can be neglected due to smallness of motor temperature T_m, and the solution has the form

$$M_b=\frac{p_{\text{on}}m_f}{p_{\text{off}}}\left\{1-\exp\left[-\frac{p_{\text{off}}}{V_0}\left(S+\frac{l}{2}\right)\right]\right\}. \tag{38}$$

Typically, the distance a motor travels on a microtubule between binding and unbinding is much less than the length of a tubule, or $p_{\text{off}}V_0^{-1}l\gg 1$, so the density saturates very quickly to the equilibrium value $M_e=p_{\text{on}}p_{\text{off}}^{-1}m_f$. This solution corresponds to a constant flux J of motors along the tubule in the gas phase,

$$J_{\text{gas}}=V_0M_e=\frac{V_0p_{\text{on}}m_f}{p_{\text{off}}}. \tag{39}$$

In the solid phase at a very low motor temperature T_m, the motor density is very close to M_0. Thus, at the end of the tubule, the flux of motors is equal to the number of motors leaving the tubule in a unit time $p_{\text{end}}M_0$. According to Eq. (37), the flux of motors J in the solid phase is a linear function of the coordinate,

$$J_{\text{solid}}=p_{\text{end}}l_0M_0+[p_{\text{off}}M_0-p_{\text{on}}m_f]\left(\frac{l}{2}-S\right). \tag{40}$$

The two phases are separated by a narrow interface (the width of the interface vanishes when motor temperature $T_m\to 0$) whose position S_0 is determined by equating these two fluxes, $J_{\text{gas}}=J_{\text{solid}}$,

$$\frac{V_0p_{\text{on}}m_f}{p_{\text{off}}}=p_{\text{end}}l_0M_0+[p_{\text{off}}M_0-p_{\text{on}}m_f]\left(\frac{l}{2}-S_0\right). \tag{41}$$

This yields the following expression for the interface position:

$$S_0=\frac{l}{2}+\frac{p_{\text{end}}l_0M_0-V_0p_{\text{on}}p_{\text{off}}^{-1}m_f}{p_{\text{off}}M_0-p_{\text{on}}m_f}. \tag{42}$$

Obviously, interface position S_0 grows with the increase of detachment probability p_{end}, and at $p_{\text{end}}=V_0p_{\text{on}}m_f[p_{\text{off}}l_0M_0]^{-1}$, we obtain $S_0=l/2$, i.e., the solid phase disappears.

Thus, the bound motor density M_b is approximately described by the following step function:

$$M_b(S)\approx M_e+(M_0-M_e)\Theta(S-S_0). \tag{43}$$

The inhomogeneous distribution of bound motors directly leads to the anisotropy of the collision rate. The coordinates along the microtubules $S_{1,2}$ are related to the positions $\mathbf{r}_{1,2}$ of the center of microtubules as follows:

$$S_{1,2}=\mathbf{n}_{1,2}\cdot(\mathbf{r}-\mathbf{r}_{1,2}). \tag{44}$$

The probability of two intersecting tubules to be linked by a motor given that they intersect W_l, which enters Eq. (32), is proportional to the bound motor concentration

$$\bar{W}_l=g_0[M_b(S_1^0)+M_b(S_2^0)], \tag{45}$$

where $S_{1,2}^0$ are the values of $S_{1,2}$ at the intersection point, and g_0 is a proportionality constant ("linking rate").

Excluding $\mathbf{r}$ from Eq. (44), one obtains

$$S_1^0=\frac{(\mathbf{r}_1-\mathbf{r}_2)[\mathbf{n}_2-\mathbf{n}_1(\mathbf{n}_1\cdot\mathbf{n}_2)]}{1-(\mathbf{n}_1\cdot\mathbf{n}_2)^2}$$

$$S_2^0=-\frac{(\mathbf{r}_1-\mathbf{r}_2)[\mathbf{n}_1-\mathbf{n}_2(\mathbf{n}_1\cdot\mathbf{n}_2)]}{1-(\mathbf{n}_1\cdot\mathbf{n}_2)^2}. \tag{46}$$

Nonuniform bound motors density $M_b(S)$ produce anisotropy: $p_l(\mathbf{r}_1,\mathbf{n}_1,\mathbf{r}_2,\mathbf{n}_2)\neq p_l(\mathbf{r}_1,\mathbf{n}_2,\mathbf{r}_2,\mathbf{n}_1)$. However, the collision rate, Eq. (45), with the stepwise expressions for $S_{1,2}^0$, (43), is awkward and impractical for further calculations. In Sec. IV, we will not use the exact form (32) with Eq. (45) as a kernel in the master equation, but will replace it with a more simple form that nevertheless, retains the main features of (32) and (45), namely, localization and anisotropy,

$$W\approx W_0(\mathbf{r}_1-\mathbf{r}_2)[1-\beta l^{-1}(\mathbf{r}_1-\mathbf{r}_2)\cdot(\mathbf{n}_1-\mathbf{n}_2)], \tag{47}$$

where the symmetric part of the kernel W_0 is of the Gaussian form

$$W_0(\mathbf{r})=\frac{g_0m}{\pi b^2}\exp\left[\frac{-\mathbf{r}^2}{b^2}\right] \tag{48}$$

with the spatial scale $b\approx l/2$, and m the total motor concentration. The dimensionless parameter β characterizes the collision rate anisotropy. The interaction kernel in this from was proposed by us on the symmetry grounds in Ref. [17].

Although the form (47) cannot be rigorously derived from (32) and (45), the anisotropy coefficient β as a function of kinetic parameters can be estimated from the expression (43). First of all, we approximate the step function in Eq. (43) by the linear function

$$M_b(S)\approx\bar{M}+\bar{\alpha}S, \tag{49}$$

where the mean motor density $\bar{M}$ and mean slope $\bar{\alpha}$ are calculated by the least mean square method using Eq. (43),

$$\bar{M}=\frac{1}{l}\int_{-l/2}^{l/2}M_bdS=\frac{M_0+M_e}{2}+(M_0-M_e)\frac{S_0}{l}$$

$$\bar{\alpha}=\frac{12}{l^3}\int_{-l/2}^{l/2}M_bSdS=6\frac{M_0-M_e}{l^3}\left(\frac{l^2}{4}-S_0^2\right). \tag{50}$$

To evaluate the effective kernel we substitute Eq. (49) into Eq. (45) and using relations (46), obtain

$$g \approx g_0[2\bar{M} + \bar{\alpha}(S_1^0 + S_2^0)] = g_0\left(2\bar{M} - \bar{\alpha}\frac{(\mathbf{r}_1 - \mathbf{r}_2)(\mathbf{n}_1 - \mathbf{n}_2)}{1 - \mathbf{n}_1\mathbf{n}_2}\right). \tag{51}$$

As one sees from Eq. (51), it coincides with phenomenological kernel Eq. (47) up to the factor $(1-\mathbf{n}_1\mathbf{n}_2)$ in the denominator. The value of the dimensionless kernel anisotropy is then

$$\beta = \frac{\bar{\alpha}l}{2\bar{M}}. \tag{52}$$

Assuming that the density in the solid phase M_0 is much larger than the density in the gas phase M_e, $\mu = M_0/M_e \gg 1$, we obtain the following estimate for the anisotropy β for $p_{\text{end}} \to 0$:

$$\beta \approx 3\left(\frac{1}{2} - \frac{S_0}{l}\right) = 3\frac{V_0 - p_{\text{end}}\mu l_0}{l p_{\text{off}}\mu}. \tag{53}$$

The anisotropy is maximum for $p_{\text{end}}=0$ ($\beta \approx V_0/p_{\text{off}}l\mu$) decreases with the increase of p_{end} and vanishes (at this approximation) at $p_{\text{end}} = V_0/\mu l_0$.

We can estimate the kernel anisotropy parameter β for different type of motors using the data from Refs. [4,5]. The parameters for kinesin and NCD are $V=1\ \mu$/s, $p_{\text{on}} = 0.4\ \mu\text{ms}^{-1}$, $p_{\text{off}}=0.5\ \text{s}^{-1}$, and $p_{\text{end}}=70\ \text{s}^{-1}$ for kinesin and $p_{\text{end}}=2.5\ \text{s}^{-1}$ for NCD. Here, $d_0 \approx 2l_0 = 20$ nm is the diameter of the microtubule, Projected (two-dimensional) density of free motors m_f in Refs. [4,5] was taken $m_f = 0.05-2\ \mu\text{m}^{-2}$. For the linear density of bound motors we obtain $M_e = p_{\text{on}}m_f/p_{\text{off}}$ and $M_0 = 1/l_0$. For parameter μ obtain $\mu = M_0/M_e = p_{\text{off}}/(l_0 p_{\text{on}} m_f) \approx 10-500 \gg 1$. Thus, for NCD-like motors when $l_0\mu p_{\text{end}} \ll 1$ we obtain the anisotropy parameter β (depending on the density ratios μ)

$$\beta_{\text{NCD}} \approx \frac{3V_0}{l p_{\text{off}}\mu} \approx 10^{-3}, \cdots, 10^{-1}. \tag{54}$$

It follows from Eq. (54) that the kernel anisotropy β increases with the increase of the concentration of free motors. Correspondingly, since for kinesin parameters probability of detachment at the end of microtubule $p_{\text{end}} > V_0 p_{\text{on}} m_f [p_{\text{off}} l_0 M_0]^{-1}$ and no solid phase is formed, the anisotropy coefficient β is essentially zero.

In this section, we considered only one mechanism contributing to the kernel anisotropy: inhomogeneous distribution of bound motors. Possibly there are other mechanisms affecting the anisotropy of the interaction, for example, finite bending rigidity of the microtubules may also contribute to both the collision rules and the collision rate. However, we leave this interesting topic to further studies.

IV. CONTINUUM DESCRIPTION OF MOTOR-MEDIATED TUBULE ORDERING

In this section, we will derive from master equation (12) continuum equations for coarse-grained local orientation $\boldsymbol{\tau}$ and density ρ using the results for interaction kernel derived in Sec. III. After integration over the δ functions, Eq. (12) assumes the form

$$\frac{\partial P}{\partial t} = D_r\frac{\partial^2 P}{\partial \phi^2} + \partial_i D_{ij}\partial_j P + Z_0 + \beta Z_1, \tag{55}$$

where nonlinear terms

$$Z_0 = \int d\mathbf{r}_1 \int_{-\phi_0}^{\phi_0} dw\{2W_0[2(\mathbf{r}_1 - \mathbf{r})]P(\mathbf{r}_1, \phi + w\gamma, t) \times P[2\mathbf{r} - \mathbf{r}_1, \phi + w(\gamma - 1), t] - W_0(\mathbf{r}_1 - \mathbf{r})P(\mathbf{r}, \phi, t) \times P(\mathbf{r}_1, \phi - w, t)\} \tag{56}$$

and

$$Z_1 = \int d\mathbf{r}_1 \int_{-\phi_0}^{\phi_0} dw\{2W_0[2(\mathbf{r}_1 - \mathbf{r})](\mathbf{r}_1 - \mathbf{r}) \cdot (\mathbf{n}_1 - \mathbf{n}) \times P(\mathbf{r}_1, \phi + w\gamma, t)P[2\mathbf{r} - \mathbf{r}_1, \phi + w(\gamma - 1), t] - W_0(\mathbf{r}_1 - \mathbf{r})(\mathbf{r}_1 - \mathbf{r}) \cdot (\mathbf{n}_1 - \mathbf{n})P(\mathbf{r}, \phi, t)P(\mathbf{r}_1, \phi - w, t)\} \tag{57}$$

are generated by the collision integral in Eq. (12).

In generic situation, Eq. (12) cannot be formally simplified because of the absence of obvious small parameter for expansion. Moreover, derivation of hydrodynamic-type equations and moments expansion used in Refs. [14,16] is not justified due to absence of apparent scale separation between the size of microtubule and the scale of the pattern (typically in experiment the scale of vortices and asters is comparable with size of the one microtubules). However, significant simplification of Eq. (12) is possible at the threshold of orientation instability, i.e., for small values of parameter ϵ. For $\epsilon \sim (\rho - \rho_c) \ll 1$, one has formally separation between the microscopic scale (a size of a microtubule l) and the macroscopic scale (typical wavelength of the orientational instability $L_i \sim l/\sqrt{\epsilon} \gg l$).

To proceed, we again perform the Fourier expansion, Eq. (6), of the probability distributions in ϕ and truncate the series at $|k| > 2$. Now $2\pi P_0$ gives the local number density $\rho(\mathbf{r}, t)$, and $P_{\pm 1}$ the local orientation $\boldsymbol{\tau}(\mathbf{r}, t)$. Deriving "amplitude equations" for ρ and $\boldsymbol{\tau}$ involves keeping only the lowest-order terms in gradients of coarse-grained density ρ and orientation $\boldsymbol{\tau}$ with respect to small parameter ϵ, (this derivation is similar to a derivation of Ginzburg-Landau-type amplitude equations from generic system of partial differential equation at the threshold of a supercritical bifurcation; see, e.g., [31]). For the details of this derivation, see [19]. The integration of the diffusion term in Eq. (55) generates linear terms, and the nonlinear "collision integrals" Z_0, Z_1 lead to nonlinear terms in the corresponding equations for $\rho, \boldsymbol{\tau}$. In rescaled variables (we normalize time by D_r and space coordinates by l), we arrive at the set of equations for the local density $\rho = g_0 m \int_0^{2\pi} P d\phi$ and orientation $\boldsymbol{\tau} = g_0 m (2\pi)^{-1} \int_0^{2\pi} \mathbf{n} P d\phi$,

$$\partial_t \rho = \nabla^2\left[D_\rho \rho - \frac{B^2\rho^2}{16}\right] - \frac{\pi B^2 H}{16}[3\nabla \cdot (\boldsymbol{\tau}\nabla^2\rho - \rho\nabla^2\boldsymbol{\tau}) + 2\partial_i(\partial_j\rho\partial_j\tau_i - \partial_i\rho\partial_j\tau_j)] - \frac{7\rho_0 B^4}{256}\nabla^4\rho \tag{58}$$

$$\partial_t \boldsymbol{\tau} = D_{\tau 1}\nabla^2\boldsymbol{\tau} + D_{\tau 2}\nabla(\nabla\cdot\boldsymbol{\tau}) + 0.273(\rho-\rho_c)\boldsymbol{\tau} - A_0|\boldsymbol{\tau}|^2\boldsymbol{\tau} - H\left[\frac{\nabla\rho^2}{16\pi} - \left(\pi-\frac{8}{3}\right)\boldsymbol{\tau}(\nabla\cdot\boldsymbol{\tau}) - \frac{8}{3}(\boldsymbol{\tau}\nabla)\boldsymbol{\tau}\right] + \frac{B^2\rho_0}{4\pi}\nabla^2\boldsymbol{\tau}, \tag{59}$$

where $D_\rho=(D_\parallel+D_\perp)/2D_r l^2=1/32$, $D_{\tau 1}=(D_\parallel+3D_\perp)/4D_r l^2=5/192$, $D_{\tau 2}=(D_\parallel-D_\perp)/2D_r l^2=1/96$. We introduced dimensionless parameters $B=b/l$ characterizing the width of the interaction kernel and $H=\beta b^2/l^2$ characterizing normalized strength of anisotropy of interaction [see Eqs. (47) and (48)]. Equations (58) and (59) generalize Eq. (10) for the case of spatially localized coupling. We assume that the density variations are small. That allows us to linearize the last two terms in Eqs. (58) and (59) near the mean density $\rho_0=\langle\rho\rangle$; otherwise, more complicated expressions given in [19] are needed. The last term in Eq. (58) regularizes the shortwave instability when the diffusion term changes sign at the density $\rho_0>\rho_b=1/4B^2$. This instability leads to strong density variations associated with formation of dense microtubule bundles (see Figs. 5 and 6 below), which is also observed experimentally for large density of molecular motors.

A. Stability of asters and vortices

If $B^2H\ll 1$, i.e., weak kernel anisotropy, the density modulations are rather small, and Eq. (59) for orientation $\boldsymbol{\tau}$ decouples from Eq. (58). It is convenient to rewrite Eq. (59) for complex variable $\chi=\tau_x+i\tau_y$ (note that it coincides with P_1^* introduced earlier in Sec. II C)

$$\partial_t\chi = \epsilon\chi - A_0|\chi|^2\chi + D_1\nabla^2\chi + D_2\bar{\nabla}^2\chi^* + H\left[\left(\pi-\tfrac{8}{3}\right)\chi\mathrm{Re}\bar{\nabla}\chi^* + \tfrac{8}{3}(\mathrm{Re}\chi^*\bar{\nabla})\chi\right], \tag{60}$$

where operator $\bar{\nabla}=\partial_x+i\partial_y$, and the diffusions $D_1=1/32+\rho_0B^2/4\pi$, $D_2=1/192$. Equation (60) is similar to the generalized Ginzburg-Landau equation known in the context of superconductivity, superfluidity, nonlinear optics, and pattern formation; see, e.g., [31]. Let us focus on the structure and the dynamics of radially symmetric solutions of (60), which can be sought in polar coordinates r, θ in the following generic form:

$$\chi = \sqrt{A_0/\epsilon}A(k\bar{r})\exp(i\theta), \tag{61}$$

where the complex amplitude $A(\bar{r})=\Phi(\bar{r})\exp[i\varphi(\bar{r})]$, and the amplitude $\Phi(\bar{r})$ and phase $\varphi(\bar{r})$ are real functions of the rescaled distance from the center $\bar{r}\to r/\sqrt{\epsilon}$. The solution with phase $\varphi(\bar{r})=0$, π corresponds to an aster, and the solution with phase $\varphi(\bar{r})\neq 0,\pi$ describes a vortex; see Fig. 4. Transitions between asters and vortices can be examined in the framework of a one-dimensional problem for the complex variable $A(r)$,

$$\partial_{\bar{r}}A = D_1\Delta_{\bar{r}}A + D_2\Delta_{\bar{r}}A^* + (1-|A|^2)A + H\left(a_1A\,\mathrm{Re}\,\nabla_{\bar{r}}A + a_2\partial_{\bar{r}}A\,\mathrm{Re}\,A + \frac{ia_2A\,\mathrm{Im}\,A}{\bar{r}}\right) \tag{62}$$

with the following differential operators:

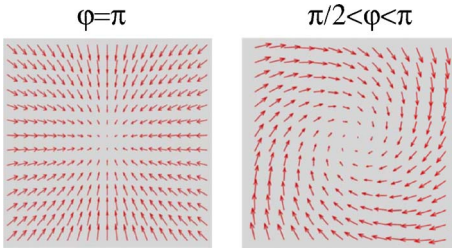

FIG. 4. (Color online) Schematic representation of orientation fields $\boldsymbol{\tau}$ for three different values of φ: aster ($\varphi=\pi$), generic vortex ($\pi/2<\varphi<\pi$), and ideal vortex ($\varphi=\pm\pi/2$).

$$\Delta_{\bar{r}}=\partial_{\bar{r}}^2+\bar{r}^{-1}\partial_{\bar{r}}-\bar{r}^{-2};\quad \nabla_{\bar{r}}=\partial_{\bar{r}}+\bar{r}^{-1} \tag{63}$$

and parameters

$$a_1=\left(\pi-\tfrac{8}{3}\right)/\sqrt{A_0}\approx 0.321,\quad a_2=\tfrac{8}{3}\sqrt{A_0}\approx 1.81$$

In Eq. (62), we also rescaled the time variable $\bar{t}\to t/\epsilon$.

The aster and vortex solutions obtained by numerical integration of Eq. (62) for certain parameter values are found in [17]. Vortices exist only for small values of kernel anisotropy H and give way to asters for larger kernel anisotropy H or larger density ρ. For $H=0$, Eq. (62) reduces to a form that was studied in [32]. It was shown in [32] that the term $\Delta_{\bar{r}}A^*$ favors (ideal) vortex solution with the phase $\varphi=\pm\pi/2$. In contrast, terms proportional to H select asters with the phase $\varphi=\pi$ (aster for the phase $\varphi=0$ is unstable for the anisotropy parameter $H>0$). Note that the phase $\varphi=\pi$ corresponds to asters with the direction of arrows toward the center, as it is shown in Fig. 4. Since we associated the direction of the vector τ with the direction of motion of molecular motors along the microtubules, the aster with the phase $\varphi=\pi$ corresponds to the experimental situation: motor moves toward the center of the aster. Increasing H leads to gradual reduction of φ, and at a finite $H_0(\rho_0)$, $\phi(r)=\pi$, i.e., the transition from vortices to asters occurs [33]. For $0<H<H_0$, the vortex solution has a nontrivial structure. We obtained that the phase $\varphi\to\pi$ for $\bar{r}\to\infty$, i.e., vortices and asters become indistinguishable far away from the core [17]. This result is consistent with the experimental observations by Surrey *et al.* [5], where it was found that the tilt angle of microtubules decreases with the increase of the distance from the vortex core.

The transitions between asters and vortices can be studied in the framework of linearized Eq. (62). For this purpose, the solution to Eq. (62) can be sought in the form

$$A(\bar{r}) = \Phi(\bar{r}) + iw(\bar{r})\exp(\lambda t), \tag{64}$$

where small real perturbation w obeys a linear equation $\hat{L}=\lambda w$ with operator

$$\hat{L}\equiv\bar{D}\Delta_{\bar{r}} + (1-\Phi^2+a_1H\nabla_{\bar{r}}\Phi) + a_2H\Phi\nabla_{\bar{r}} \tag{65}$$

($\bar{D}=D_1-D_2$) with zero boundary conditions at $\bar{r}=0,\infty$. This eigenvalue problem can be solved by the matching-shooting method. A positive eigenvalue λ corresponds to the emergence of a nonzero phase $\varphi(\bar{r})$, i.e., a vortex.

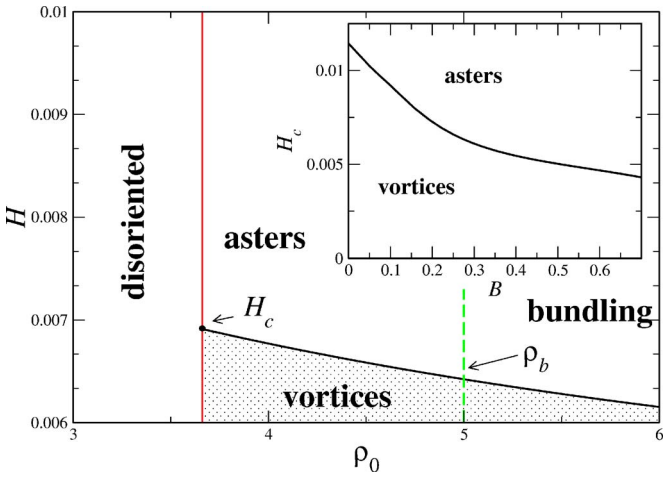

FIG. 5. (Color online) Phase boundaries obtained form the linear stability analysis of the aster solution for $B^2=0.05$. Dashed line shows bundling instability limit $\rho_0=\rho_b=5$. Inset: Position of critical point H_c vs B at $\rho_0=4.5$.

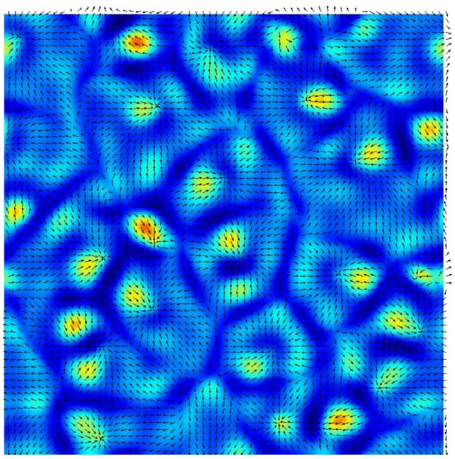

FIG. 6. (Color online) Composite image of the density and orientation (arrows) fields in the regime of density instability. Density changes from $\rho_{\max}\approx 10$ [bright (red online)] to $\rho_{\min}\approx 4$ [black (dark blue online)]. Parameters: $B^2=0.05$, $\rho_0=6$, $H=0.125$, domain of integration 80×80 units.

The resulting phase diagram of the continuum model (58) and (59) is shown in Fig. 5. The solid line $H_0(\rho_0)$ separating vortices from asters is obtained from the solution of the linearized Eq. (62) by tracking the most unstable eigenvalue λ of the aster. The dashed line corresponds to the onset of the orientation instability, $\rho_0=\rho_c$. The lines meet at the critical point $H_c=H_0(\rho_c)$ above which vortices are unstable for arbitrary small $\epsilon>0$. The phase diagram is qualitatively consistent with experiments; see Ref. [5]: for low value of kernel anisotropy $H<H_c$ (which according to our estimates in Sec. III B corresponds to kinesinlike motors with very small anisotropy value β), increase of the density ρ_0 first leads to formation of vortices and then asters. For $H>H_c$ (which apparently corresponds to NCD motors with large anisotropy) only asters are observed. As we mentioned above, for large density $\rho_0>\rho_b=1/4B^2$, in addition to orientation instability Eq. (58) describes a densityinstability when the nonlinear diffusion term [first term in the right-hand side of Eq. (58)] changes sign. Numerical studies of the full system [(58) and (59)] indeed demonstrate formation of extended domains of high density not associated with the asters; see Fig. 6. Although our model (58) and (59) yields the density instability and bundle formation in accordance with experiment, we anticipate only qualitative agreement in this regime because the model itself is derived in the low-density limit when only binary interactions are included.

B. Interaction of asters and vortices

For $H\neq 0$ well-separated vortices and asters exhibit exponentially weak interaction. For asters it follows from the fact that $\hat{L}$ is not a self-adjoint operator. To investigate the interaction between asters, we need to examine the asymptotic null space of the adjoint operator $\hat{L}^\dagger$ for $\bar{r}\to\infty$ (see, for details, [31]). After simple algebra, we obtain that for $\bar{r}\to\infty$ the adjoint operator is of the form

$$\hat{L}^\dagger \equiv \bar{D}\partial_{\bar{r}}^2 - a_2 H\partial_{\bar{r}}. \tag{66}$$

Substituting the solution to the equation $\hat{L}^\dagger w^\dagger=0$ in the form $w^\dagger\sim\exp[\bar{p}\bar{r}]$, we obtain that there are two solutions: $\bar{p}=0$, which describes the neutral translation mode, and the nontrivial solution,

$$\bar{p}=a_2 H/\bar{D}. \tag{67}$$

Since because to interaction the well-separated asters produce only small perturbations to their shape, these perturbations can be treated in linear approximation, and the exponent (67) characterizes asymptotic screening of the interaction between the asters analogous to the interaction of spiral waves in the Ginzburg-Landau equation; see Ref. [31] for details of analysis. Thus, we obtain that perturbations produced due to interaction of well-separated asters decay as $w\sim\exp[-\bar{r}/L_0]$ with the screening length $L_0=1/\bar{p}$, or in original units $L_0=\bar{D}/a_2H\sqrt{\epsilon}=\bar{D}/a_2H\sqrt{\rho/\rho_c-1}$ (see, for details, [31]). Screening length L_0 diverges for $H\to 0$ and at the threshold density $\rho_0\to\rho_c$. Similar analysis can be performed for vortices. This analysis implies that two well-separated asters or vortices will experience drift with the velocity V_{12} of the order $V_{12}\sim\exp[-r_{12}/L_0]$, where $r_{12}$is the distance between centers of asters or vortices.

C. Numerical solution of full system

We also studied the full system [(58) and (59)] numerically. Integration was performed in a two-dimensional square domain with periodic boundary conditions by the quasispectral method. For small kernel anisotropy H, we observed vortices and for larger H asters, in agreement with the above analysis. Since vortices exist for smaller values of H, their screening length L_0 is larger than for the asters because $L_0\sim 1/H$; see Eq. (67). Thus, the vortices interact more strongly and are more keen to annihilate than asters. Asters

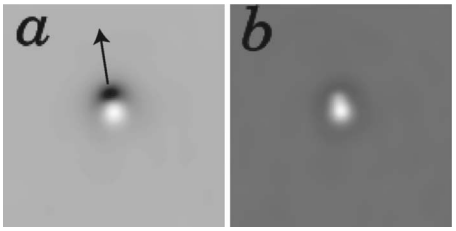

FIG. 7. Gray-coded images illustrating drift instability of asters for $H=0.125$, $B=0.06$, $\rho_0=4$, size of the image 40×40 at the moment of time $t=300$. Left image shows $|\boldsymbol{\tau}|$, right image shows ρ, arrow indicates the direction of drift. Color code: black corresponds to zero, white corresponds to maximum.

have a unique orientation of the microtubules (here, toward the center). Asters with the opposite orientation of $\boldsymbol{\tau}$ are unstable [see Figs. 5(a) and 5(b) of Ref. [17]].

In large domains, asters form a disordered network of cells with the cell size of the order of screening length L_0. Neighboring cells are separated by the "shock lines" terminated by saddle-type defects. The pattern of asters resembles a "frozen" glass state of spirals observed in the complex Ginsburg-Landau model [31,34]. Starting from a random initial condition we observed initial merging and annihilation of asters. Eventually, annihilation slows down due to exponential weakening of the interaction of asters. For the same integration time, the number of vortices is typically smaller than the number of asters because the screening length of asters is smaller.

D. Drift instability of the asters

In experiments [4,5], asters often are not stationary; they drift and coalesce. Surprisingly, in our numerical investigations of Eqs. (58) and (59) we also observed that typically the center of an aster is unstable and develops a spontaneous acceleration instability, see Fig. 7. This instability is reminiscent of the instability of spiral wave cores in the complex Ginzburg-Landau equation in a large dispersion limit; see Ref. [35]. This instability was associated in Ref. [35] with the exponential growth of localized mode in the form $w_1(r)\exp[i\theta]$ that results in the core displacement.

Although this instability may indeed be the cause of experimentally observed aster drift, other mechanisms (such as gradients of microtubules or motor distributions, effects of the boundaries, etc.) cannot be excluded. Furthermore, it cannot also be excluded that this drift instability is an artifact of the approximations made in derivation of amplitude equations (58) and (59). Truncated higher-order terms can, in principle, suppress this instability in the experimentally relevant range of parameters. For example, we were able to suppress the instability artificially increasing the prefactor before the $\nabla^4\rho$ term in Eq. (58). More detailed experiments are needed to determine stability of the asters and vortices. To study the drift instability numerically, we prepared an initial condition in the form of an axisymmetric aster solution perturbed by a small amplitude noise. In the course of motion the solution breaks the axial symmetry, typical structure of the moving aster is shown in Fig. 7. There is a small

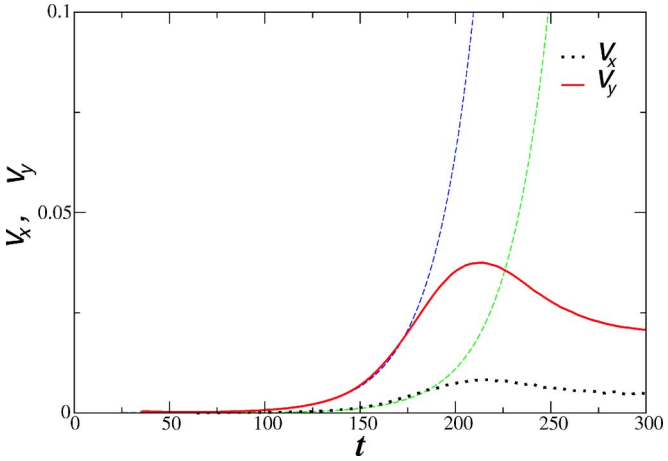

FIG. 8. (Color online) Components of aster core velocity $\mathbf{V}_a=(V_x,V_y)$ vs time t for parameters of Fig. 7. Solid line shows V_y, dotted line shows V_x, and dashed lines depict exponential fit $V_{x,y}\sim\exp(\lambda t)$ for the first 150 units of time.

but noticeable ($\sim10\%$) increase of the density ρ and the amplitude of orientation $|\boldsymbol{\tau}|$ behind the aster, for the immobile solution the position of the zero of $\boldsymbol{\tau}$ and maximum of ρ coincides. The instability accelerates collisions and coalescence of asters. However, the growth rate λ of the instability appears to be very small and aster solutions are well preserved for a very long time (several hundreds of dimensionless units). Figure 8 shows the velocity of aster core $\mathbf{V}_a$ vs time for the parameters of Fig. 7. One clearly sees initial exponential growth of the aster velocity.

V. EFFECTS OF MOTORS ATTACHED TO THE BOTTOM PLATE

In previous sections, we considered microtubules interacting with molecular motors freely floating in the solvent. However, in in vitro experiments it is difficult to prevent attachment of some fraction of motors to the bottom of the cell with one of their two heads. The other (free) head of the attached (absorbed) molecular motor then may bind to a microtubule and push it in the direction opposite its orientation. This effect was observed experimentally in Ref. [36] (referred to as microtubule gliding assays). Recently, the dynamics of microtubules interacting with attached motors (however, without free motors) was studied in Ref. [37].

The effect of attached motors can be easily incorporated in the master equation

$$\frac{\partial P}{\partial t}=D_r\frac{\partial^2 P}{\partial\phi^2}+\partial_i D_{ij}\partial_j P+\alpha\nabla\cdot(\mathbf{n}P)+Z_0+Z_1. \quad (68)$$

Here α is the fraction of the attached motors, and the term $\nabla\cdot(\mathbf{n}P)$ accounts for the transport of microtubules in the direction opposite to their orientation vector $\mathbf{n}=[\cos\phi,\sin\phi]$. The terms $Z_{0,1}$ remain unchanged. It is easy to check that the drift term will generate additional linear terms $\alpha\pi\nabla\boldsymbol{\tau}$ in Eq. (58) and $\alpha(4\pi)^{-1}\nabla\rho$ in Eq. (59).

It is useful to write Eq. (58) in the form of the mass conservation law

$$\rho_t = -\nabla \mathbf{J} \tag{69}$$

with the corresponding mass flux $\mathbf{J}$. The anisotropic part of the kernel generates mass flux, which is second order in the gradients of $\rho, \boldsymbol{\tau}$. In the lowest order, flux $\mathbf{J} \sim \alpha \boldsymbol{\tau}$ due to the interaction of tubules with motors attached by one head to the substrate [37]. This makes the dynamics similar to that of self-propelled particles; see, e.g., [32]. Without attachment to substrate (the situation considered previously in Sec. IV) this term is prohibited by the momentum conservation: molecular motors produce only internal forces which cannot displace the center of mass of the system. In Ref. [16], a similar contribution to the flux was attributed to the net displacement of the center of the microtubule pair due to the anisotropy of the viscous drag coefficient. However, this pure hydrodynamic effect is probably smaller than the advection produced by the motors absorbed at the substrate.

Although the fraction of absorbed motors α might be small, it still can produce a considerable effect because it generates the lowest-order transport term in Eqs. (58) and (59). Numerical studies of Eqs. (58) and (59) with additional α terms reveal that qualitative features are not very sensitive to the presence of these terms for small $\alpha \ll 1$, as long as the diffusive transport in the equation for the density ρ dominates advection. However, for moderate α values we observed that asters and vortices become even less localized; see Fig. 9. This delocalization is because the absorbed motors advect the microtubules in the direction opposite to their orientation. Consequently, these motors move the tubules *from the asters* and make a small depression of density for $\alpha \neq 0$ contrary to the density peak for $\alpha = 0$, compare images in Fig. 9. Similar results were also obtained for vortices. Remarkably, the suppression of density of microtubules in the core of vortex is also observed experimentally; see Fig. 2(a) in Ref. [5].

The presence of motors attached to the substrate may also explain differential rotation of vortices absent in our previous analysis. Indeed, since these motors generate net motion of individual microtubules with the velocity $\sim \alpha$, they can support rotating configurations similar to those observed in the system of vibrated rods [32]. Obviously, no rotation anticipated for asters due to pure radial orientation of microtubules: the forces induced by motors attached to substrate will be compensated by "pressure" gradient due to redistribution of density of microtubules. In contrary, the rotation is present for vortices. Far away from the core, the distinction between vortex and aster disappears and the rotation is localized only at the core of the vortex where the phase ϕ is different from π. Since the amplitude of orientation vector τ grows almost linearly from the vortex core and reaches asymptotic value $\tau_0 \approx \sqrt{\epsilon / A_0}$ at the distance of about 1–2 dimensionless units, the rotation frequency of the vortex core $\omega \approx \alpha \tau_0$. Indeed, rotation of the vortex core was observed experimentally. For the parameters of our numerical studies, the frequency ω is very small due to the smallness of $\alpha = 0.004$; thus, during the time of numerical experiment (<1000 dimensionless units of time) the vortex core turned only the fraction of full circle.

VI. INHOMOGENEOUS DISTRIBUTION OF MOTORS

In previous sections, we assumed a homogeneous bulk distribution of molecular motors (however, we took into account local inhomogeneity of bound motor concentration on the scale of a single tubule to account for the collision rate anisotropy in Sec. III B). This assumption was justified by the fact that the diffusion of motors is about two orders of magnitude larger than of microtubules. However, experiments indicate that even despite this strong diffusion, molecular motors aggregate in the core regions of asters and vortices due to the directed transport of motors by microtubules [7]. The effects of variable motor density were first considered in Ref. [9–11], and transport and accumulation of motors at the centers of asters and vortices was assumed to be a primary mechanism of self-organization. Here, we show that although the effect of variable motor density indeed improves agreement with experiment, it does not qualitatively change our previous conclusions obtained under the assumption of uniform motor density. In particular, we obtained vortices for low values of H and small motor density and asters for higher motor density.

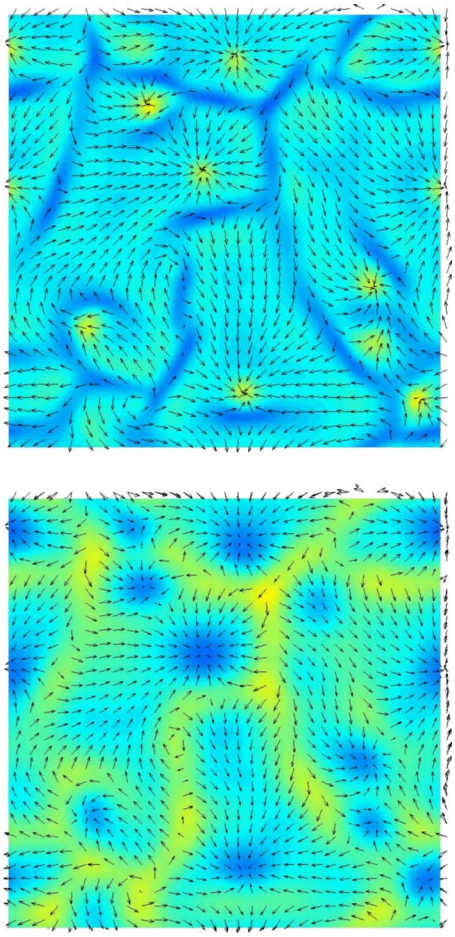

FIG. 9. (Color online) Comparison between density distributions [dark (blue online)], $\rho = \rho_{\min} \approx 3.7$, and light (yellow online), $\rho = \rho_{\max} \approx 4.4$ without drift ($\alpha = 0$, upper image) and with drift ($\alpha = 0.004$, lower image). Arrows show corresponding orientation. Parameters of integrations: $B^2 = 0.05$, $\rho_0 = 4$, $H = 0.1$, domain of integration 80×80.

To describe the dynamics of the motor concentration we again invoke the equations for free m_f and bound m_b motor concentrations, but unlike Sec. III B, we will coarse grain

these concentrations on a mesoscopic scale much larger than the size of individual filament similar to Ref. [7] (see also [9–11]). Note that instead of M_b we use the notation m_b to describe the concentration of bound motors per unit area rather than per unit length of a single motor as in Sec. III B. The concentrations m_b, m_f obey the advection-diffusion equations [7,9] (compare to Sec. III B)

$$\partial_t m_f = D\nabla^2 m_f - \rho(P_{\text{on}} m_f - P_{\text{off}} m_b)$$

$$\partial_t m_b = -\zeta \nabla m_b \boldsymbol{\tau} + \rho(P^{\text{on}} m_f - P_{\text{off}} m_b), \tag{70}$$

where P_{on}, P_{off} are the rates of binding and unbinding of motor to the microtubules, D, ζ are diffusion and advection coefficients accordingly (advection velocity $\mathbf{V}=\zeta\boldsymbol{\tau}$). Note that bulk attachment and/or detachment rates are: $P_{\text{off}}=p_{\text{off}}$ from Sec. III B, but $P_{\text{on}} \approx p_{\text{on}} d_0^{-1}$.

If we assume that the distributions of motor densities m_f, m_b are smooth and the binding and/or unbinding rates are large, then the right-hand side Eqs. (70) is dominated by the last term describing binding and/or unbinding of the motors, leading to the local balance relation between motor densities m_f, m_b

$$P_{\text{on}} m_f \approx P_{\text{off}} m_b. \tag{71}$$

Then we can reduce system (70) to a single equation for the total motor density $m=m_f+m_b$:

$$\partial_t m = D_0 \nabla^2 m - \zeta_0 \nabla m\boldsymbol{\tau} \tag{72}$$

with renormalized diffusion $D_0=DP_{\text{off}}/(P_{\text{off}}+P_{\text{on}})$ and advection rate $\zeta_0=\zeta P^{\text{on}}/(P_{\text{off}}+P_{\text{on}})$.

Accordingly, we need to modify the expression for the interaction kernel Eq. (47) in order to include the effect of motor inhomogeneity. The simplest way to include inhomogeneous motor density into the kernel is to replace the constant motor density m in the symmetric part of the interaction kernel (48) by $m[(\mathbf{r}_1+\mathbf{r}_2)/2]$. Taking the motor concentration in the middle point $(\mathbf{r}_1+\mathbf{r}_2)/2$ is necessary to preserve the mass conservation law. Repeating the calculations presented in the previous sections one can derive equations similar to Eqs. (58) and (59), but for the normalized tubule density $\rho=g_0\int_0^{2\pi} P d\phi$ that *does not* absorb the motor density m. The resulting equations are very cumbersome, especially for the transport term in Eq. (58).

One can simplify the problem considerably using the fact that the motor diffusion is high and, therefore, the distribution of total motor density m is smooth. Then, one can neglect the derivatives of m where appropriate, and the resulting equations in time rescaled by D_r and space rescaled by l assume the form

$$\partial_t \rho = \nabla^2 \left[D_\rho \rho - \frac{mB^2\rho^2}{16} \right] + \alpha\pi \nabla \boldsymbol{\tau} - \frac{\pi B^2 H}{16} [3 \nabla m(\boldsymbol{\tau}\nabla^2\rho - \rho\nabla^2\boldsymbol{\tau}) + 2\partial_i m(\partial_j\rho\partial_j\tau_i - \partial_i\rho\partial_j\tau_j)] - \frac{7\rho_0 m_0 B^4}{256}\nabla^4\rho \tag{73}$$

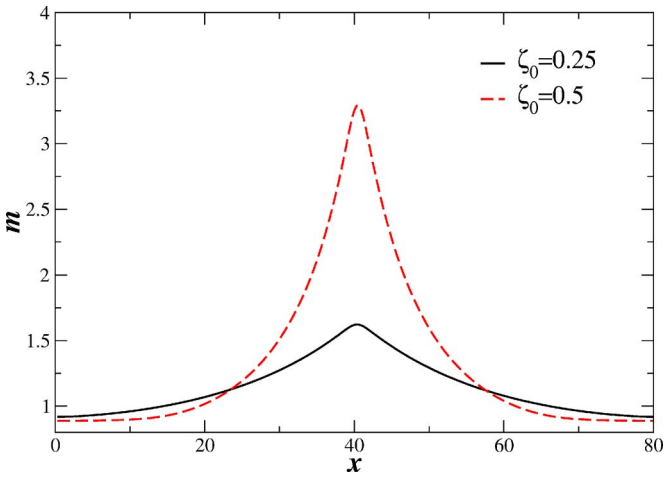

FIG. 10. (Color online) Motor concentration profiles m for an isolated aster for $H=0.125$, $B=0.06, D_0=5$, and $m_0=1$, $\rho_0=4$ and different values of motor advection ζ_0.

$$\partial_t \boldsymbol{\tau} = D_{\tau 1}\nabla^2\boldsymbol{\tau} + D_{\tau 2}\nabla(\nabla\cdot\boldsymbol{\tau}) + \frac{\alpha}{4\pi}\nabla\rho + \left[\left(\frac{4}{\pi}-1\right)m\rho - 1\right]\boldsymbol{\tau} - A_0 m^2|\boldsymbol{\tau}|^2\boldsymbol{\tau} - Hm\left[\frac{\nabla\rho^2}{16\pi} - \left(\pi - \frac{8}{3}\right)\boldsymbol{\tau}(\nabla\cdot\boldsymbol{\tau}) - \frac{8}{3}(\boldsymbol{\tau}\nabla)\boldsymbol{\tau}\right] + \frac{B^2\rho_0 m_0}{4\pi}\nabla^2\boldsymbol{\tau}. \tag{74}$$

Thus, motor density m is included in the lowest order in gradient expansion. We also included terms $\sim\alpha$ describing the transport of microtubules by the absorbed motors. Again for simplicity we replaced the motor density m by its mean value m_0 in the last terms in Eqs. (73) and (74). Although the diffusion-advection equation for the motor density [Eq. (72)] is somewhat similar to that of [9], the microscopic derivation of the coupling between all three fields: density of microtubules ρ, orientation $\boldsymbol{\tau}$, and total motor density m was not considered before.

We carried out numerical studies of Eqs. (72)–(74). The values of the motor diffusion D_0 and motor advection ξ_0 can be estimated from the experimental conditions, in our dimensionless units $D_0 \sim 1..5$ and $\xi_0 \sim 1$. Selected results are shown in Figs. 10 and 11. In agreement with experiment, we observed that motors tend to accumulate in the center of an aster or a vortex; see Figs. 10 and 11, as in [7]. Otherwise, qualitative behavior of formation of asters and vortices remains the same. As seen in Fig. 11, initial multiaster state coarsens and leads to the formation of a network of large asters separated by the domain walls.

VII. CONCLUSIONS

In this paper, we derived continuous equations for the evolution of microtubule concentration and orientation due to their interaction via molecular motors. We found that an initially disordered system exhibits an ordering instability qualitatively similar to the nematic phase transition in ordinary polymers at high density. The important difference is

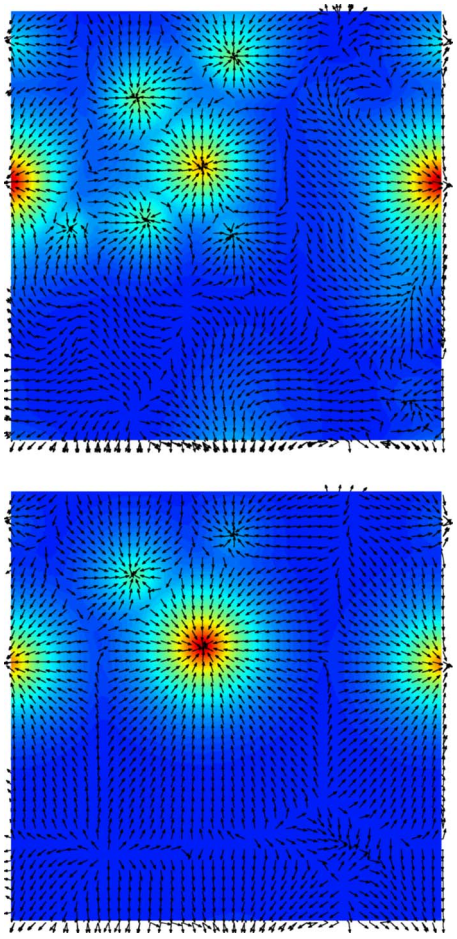

FIG. 11. (Color online) Color-coded images of density of motors at $t=200$ (left) and $t=1000$ (right). Bright (red online) corresponds to the maximum density and dark (blue online) to the minimum density, domain size is 80×80 units, $\zeta_0=0.5$, $H=0.125$, $D_0=5$, $m_0=1$. Arrows show orientation of microtubules.

that here the ordering instability is mediated by molecular motors and can occur at arbitrary low densities of microtubules. At the nonlinear stage, the instability leads to the experimentally observed formation of asters and vortices. Qualitatively similar vortices were observed in a system of interacting granular rods [32,38,39]. Although we find that it suffices to consider only the density and orientation of tubules to explain the basic phenomenology, a better agreement with experiment is obtained when we include motor density as an additional field and take into account motors attachment to the substrate [7,9,10].

Many aspects of self-assembly in microtubule-motor systems require further investigation. In particular, we anticipate that flexibility of the microtubules may have a strong effect on the details of interaction—a question that we plan to address in future work. Another interesting question is role of the hydrodynamic interaction between the microtubules and effects of fluctuations on the orientation transition. Furthermore, our theory is derived in the limit of small density of the microtubules and takes into account only binary interactions among tubules. We anticipate that multiparticle interactions may play a significant role in the dynamics in high-density regions, such as cores of asters and vortices, as well as bundles. For example, it is likely that when many microtubules are joined at the end by motors and affected by the noise, they may spontaneously form an asterlike structure. However, a description of this state goes beyond the framework of the continuum theory developed in this paper.

There are many predictions following from our analysis that possibly deserve experimental verification. For example, we find that the anisotropy of the interaction kernel is associated with the inhomogeneous density of motors along the microtubules. We observed that the motors attached to the substrate reduce the density of microtubules in the cores of asters and vortices. We predicted an acceleration instability, which leads to a drift of isolated asters. Hopefully, new generations of experiments will be able to address these issues.

Although our approach was developed for a very specific problem, molecular motors-mediated interaction of microtubules in quasi-two-dimensional geometry, we anticipate that with certain modifications it can be applied to a variety of different systems, such as rod-shaped swimming bacteria [40], vibrated granular rod systems, both polar [38,39] and apolar [41]. We believe that the concept of inelastic collisions in angle space resulting in alignment of rod directions is a primary mechanism driving self-organization in these very different systems. Moreover, it is interesting to make a connection between our approach and the generic hydrodynamic models of active "nematic" systems developed in Ref. [42].

ACKNOWLEDGMENTS

We thank Jacques Prost, Anthony Maggs, Francois Nédélec, Frank Jülicher, Karsten Kruse, Leo Kadanoff, Raymond Goldstein, Sriram Ramaswamy, Hugues Chate, Eli Ben-Naim, and Valerii Vinokur for useful discussions. This work was supported by the U.S. Department of Energy Grants No. W-31-109-ENG-38 (I.A.) and No. DE-FG02-04ER46135 (L.T.).

[1] J. Howard, *Mechanics of Motor Proteins and the Cytoskeleton* (Springer, New York, 2000).
[2] K. Takiguchi, J. Biol. Chem. **109**, 250 (1991).
[3] R. Urrutia, M. A. McNiven, J. P. Albanesi, D. B. Murphy, and B. Kachar, Proc. Natl. Acad. Sci. U.S.A. **88**, 6701 (1991).
[4] F. J. Nédélec, T. Surrey, A. C. Maggs, and S. Leibler, Nature (London) **389**, 305 (1997).
[5] T. Surrey, F. Nédélec, S. Leibler, and E. Karsenti, Science **292**, 1167 (2001).
[6] D. Humphrey, C. Duggan, D. Saha, D. Smith, and J. Käs, Nature (London) **416**, 413 (2002).
[7] F. Nédélec, T. Surrey, and A. C. Maggs, Phys. Rev. Lett. **86**,

3192 (2001).
[8] In experiments [4,5] artificial molecular constructs which couple four to eight motors using streptavidin-biotin links were used instead of isolated motors; however, it does not qualitatively change the mechanism of microtubule-motor interaction.
[9] H. Y. Lee and M. Kardar, Phys. Rev. E **64**, 056113 (2001).
[10] J. Kim, Y. Park, B. Kahng, and H. Y. Lee, J. Korean Phys. Soc. **42**, 162 (2003).
[11] S. Sankararaman, G. I. Menon, and P. B. Sunil Kumar, Phys. Rev. E **70**, 031905 (2004).
[12] K. Kruse, J. F. Joanny, F. Jülicher, J. Prost, and K. Sekimoto, Phys. Rev. Lett. **92**, 078101 (2004).
[13] R. Voituriez, J. F. Joanny, and J. Prost, Phys. Rev. Lett. **96**, 028102 (2006).
[14] T. B. Liverpool and M. C. Marchetti, Phys. Rev. Lett. **90**, 138102 (2003).
[15] This point was challenged in F. Ziebert and W. Zimmermann, Phys. Rev. Lett. **93**, 159801 (2004).
[16] T. B. Liverpool and M. C. Marchetti, Europhys. Lett. **69**, 846 (2005).
[17] I. S. Aranson and L. S. Tsimring, Phys. Rev. E **71**, 050901(R) (2005).
[18] In a recent publication, Ahmadi, Liverpool, and Marchetti, Phys. Rev. E **72**, 060901(R) (2005), modified the phenomenological expression for the rotational flux first introduced in Ref. [14] and also found the orientational instability first described in Ref. [17].
[19] See in EPAPS Document No. E-PLEEE8-74-140609 for the appendix. For more information EPAPS, see http://www.aip.org/pubservs/epaps.html
[20] E. Ben-Naim and P. L. Krapivsky, Phys. Rev. E **61**, R5 (2000).
[21] E. Ben-Naim and P. L. Krapivsky, Phys. Rev. E **73**, 031109 (2006).
[22] M. Doi and S. F. Edwards, *The Theory of Polymer Dynamics* (Clarendon Press, Oxford, 1988).
[23] A. J. Levine, T. B. Liverpool, and F. C. MacKintosh, Phys. Rev. E **69**, 021503 (2004).
[24] In the three-dimensional case, the drag coefficients $\xi_{\parallel}$, $\xi_{\perp}$ for rodlike objects are different by the factor of two [22]. However, the relative difference between $\xi_{\parallel}$ and $\xi_{\perp}$ decreases in thin fluid films and membranes [23].
[25] R. B. Case, D. W. Pierce, N. Hom-Booher, C. L. Hart, and R. D. Vale, Cell **90**, 959 (1997).
[26] In fact, realistic situation can be more complicated because motors can move on several parallel tracks along the microtubule. This will result in renormalization of the maximum closed packed density.
[27] E. L. Grossman, Tong Zhou, and E. Ben-Naim, Phys. Rev. E **55**, 4200 (1997).
[28] P. K. Haff, J. Fluid Mech. **134**, 401 (1983).
[29] J. T. Jenkins and M. W. Richman, Phys. Fluids **28**, 3485 (1985).
[30] Accumulation of motors at the polar end of microtubule was indeed observed experimentally in Ref. [25].
[31] I. S. Aranson and L. Kramer, Rev. Mod. Phys. **74**, 99 (2002).
[32] I. S. Aranson and L. S. Tsimring, Phys. Rev. E **67**, 021305 (2003).
[33] Our analysis predicts that ideal vortices with $\varphi=\pm\pi/2$ exist only $H=0$, and, therefore are not robust. For arbitrary $H\neq 0$, we obtain "generic" vortex solutions or spirals with $\varphi(r) \neq \pm\pi/2$. This result contradicts Ref. [12] where ideal vortices with $\varphi=\pm\pi/2$ were predicted to be stable in a certain domain of the phase diagram.
[34] C. Brito, I. S. Aranson, and H. Chaté, Phys. Rev. Lett. **90**, 068301 (2003).
[35] I. Aranson, L. Kramer, and A. Weber, Phys. Rev. Lett. **72**, 2316 (1994).
[36] Y. Vugmeyster, E. Berliner, and J. Gelles, Biochemistry **37**, 747 (1998); R. D. Vale, R. A. Milligan, Science **288**, 88 (2000).
[37] P. Kraikivski, R. Lipowsky, and J. Kierfeld, Phys. Rev. Lett. **96**, 258103 (2006).
[38] D. L. Blair, T. Neicu, and A. Kudrolli, Phys. Rev. E **67**, 031303 (2003).
[39] D. Volfson, A. Kudrolli, and L. S. Tsimring, Phys. Rev. E **70**, 051312 (2004).
[40] C. Dombrowski, L. Cisneros, S. Chatkaew, R. E. Goldstein, and J. O. Kessler, Phys. Rev. Lett. **93**, 098103 (2004).
[41] V. Narayan, N. Menon, and S. Ramaswamy, J. Stat. Mech.: Theory Exp. P01005 (2006).
[42] R. A. Simha and S. Ramaswamy, Phys. Rev. Lett. **89**, 058101 (2002).